Dynamics and Controls Analysis for the NGST Yardstick Concept
Part I – Design, Models and Assumptions

I. THE INTEGRATED SYSTEM-LEVEL MODEL

NGST has combined the use of mature commercial analysis codes such as FEMAP, NASTRAN, Matlab[TM] with JPL-developed tools such as IMOS [1] and MACOS [2,3] to create a highly integrated multidisciplinary analysis and simulation environment for the analysis of controls-structures-optics interaction [4]. NGST requires line-of-sight (LOS) stabilization to 5 mas, 1σ, and an RMS wavefront error (WFE) of $\lambda/14$ - 0.157 microns at 2.2 microns wavelength. The NASA "yardstick" architecture uses a fairly simple pointing control and image stabilization subsystem design featuring two control loops [5]. The first is a low bandwidth Attitude Control System loop including star trackers, gyros, reaction wheels, and a digital PID controller. The second is a high bandwidth servo loop controlling a two-axis gimballed, reactionless Fast Steering Mirror that tracks the image centroid using a guide star from the NIR science camera.. These loops must interact with a lightweight, flexible, and lightly damped structure perturbed by internal forces and torques from the conventional ball-bearing reaction wheels. A system-level block diagram of this control architecture is shown in Figure I-1, taken from the Simulink[TM] model that is the basis of the non-linear time-domain simulations employed to study the end-to-end performance.
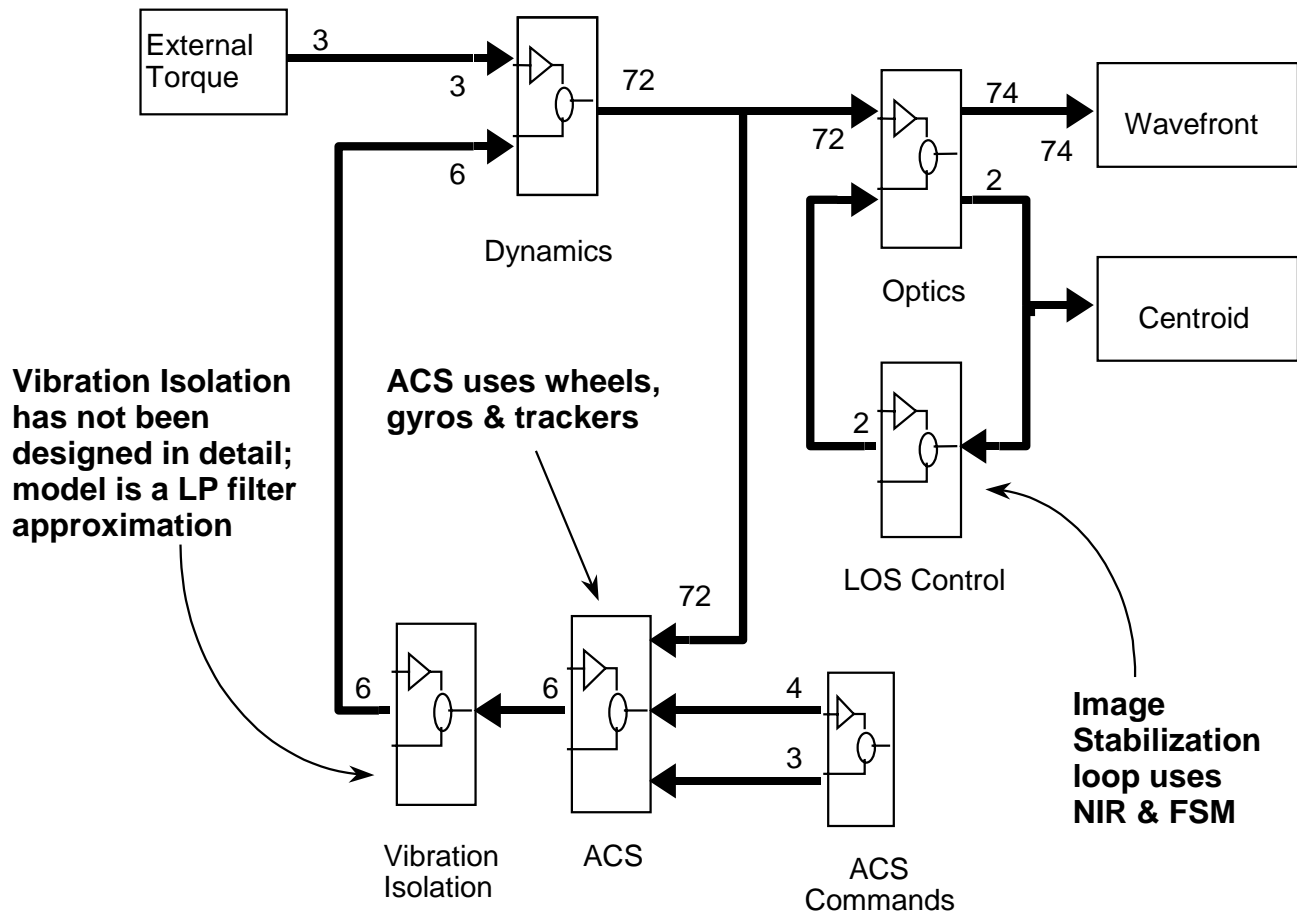

Figure I-1   Integrated Simulation Top-level Block Diagram

II. ATTITUDE CONTROL SYSTEM, REACTION WHEEL, AND VIBRATION ISOLATION MODELS

The fine pointing mode of the ACS is an adaptation of the design successfully employed on the recent Rossi X-ray Timing Explorer [6] mission. Gyros and star trackers are used as sensors for attitude determination. Attitude is maintained as a quaternion and propagated in time by the rate signals from the gyros sampled at a 10 Hz rate. The star trackers are sampled at a 2 Hz rate; these direct inertial attitude measurements are optimally combined with the gyro-propagated attitude via a Kalman Filter. Reaction wheels provide torques to steer the observatory. There are 4 wheels arranged in a pyramid-like geometry; all wheels are actively controlled to provide the 3-axis control. This allows an extra degree-of-freedom in the controller used to bias the mean wheel speed to a desired set point. This feature may be exploited to avoid structural resonances or to maximize bearing lifetime. The 3-axis torque commands are developed via a digital controller consisting of three decoupled PID contollers in series with lowpass filters for flexible mode attenuation. A block diagram of the ACS system, taken from the Simulink^{TM} time-domain simulation model, is shown in Figure II-1.

Command Rate

PID bandwidth is 0.025 Hz

Command Position

3rd order LP elliptic filters for flexible mode gain suppression

K

Estimated Inertia Tensor   Structural Filters   Wheels

Forces & Torques

gyro

Attitude Determination   PID Controllers

Wheel model includes non-linearities and imbalance disturbances

Kalman Filter blends 10 Hz IRU and 2 Hz ST data to provide optimal attitude estimate
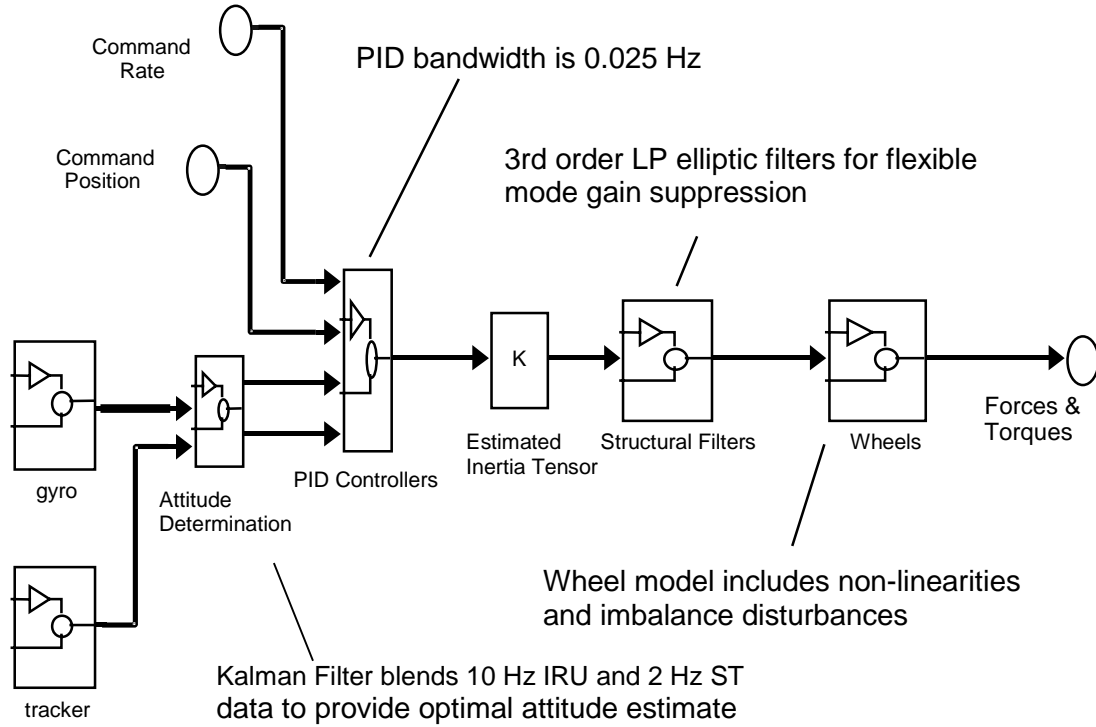
tracker

Figure II-1   ACS Block Diagram

The Kalman Filter used for attitude determination design traces its heritage to Landsat [7] and has been refined on subsequent missions such as EUVE and XTE. This filter assumes that the attitude (star tracker) and rate (gyro) measurements are corrupted by white noise, and furthermore that the rate measurements are corrupted by a random walk component (rate bias, or gyro drift). The measurement models are given by

$$\hat{\omega} = \omega + b + \eta_v \quad \eta_v \sim (0, \sigma_v) \quad \text{(rate bias, rate white noise)}$$

$$\dot{b} = \eta_u \quad \eta_u \sim (0, \sigma_u) \quad \text{(bias random walk)}$$

$$\hat{\theta} = \theta + \eta_n \quad \eta_n \sim (0, \sigma_n) \quad \text{(angle white noise)}$$

Discrete-time versions of these models are implemented in the simulation.

The inputs to the Kalman Filter are the residuals, or differences, between the measured and expected positions of guide stars. The model contains a star catalog to implement this feature. The outputs of the filter are estimated errors in the inertial attitude estimate (roll, pitch and yaw angle updates) and in the rate bias estimate (roll, pitch and yaw gyro drift updates). The predicted performance of this attitude determination system can be found by iterating the filter equations to steady-state. Although precise estimates of the filter performance require numeric simulation or covariance analysis, a useful design tool may be employed to make a first cut at key filter parameters. An analytic solution was found [8] for the case a single-axis estimation problem, where the standard deviations of the attitude and rate bias estimates are given by

$$\Delta\theta = T_u^{1/4}\sigma_n^{1/2}\left(\sigma_v^2 + 2\sigma_u\sigma_n T_u^{1/2}\right)^{1/4}$$

$$\Delta\omega = \sigma_u^{1/2}\left(\sigma_v^2 + 2\sigma_u\sigma_n T_u^{1/2}\right)^{1/4}$$

where T_u is the Kalman Filter update rate (star tracker sample rate) and the other parameters are the standard deviations of the measurement noise processes given above. Given model parameters for the Kearfott gyro flown on XTE ($\sigma_v = 0.01$ arcsec/sec$^{1/2}$, $\sigma_u = 7\text{x}10^{-5}$ arcsec/sec$^{3/2}$) and the specifications for the new Lockheed AST301 start tracker ($\sigma_n = 1.35$ arcsec/star/sample), the above solution is used to set the 2 Hz star tracker update rate. A numerical simulation of the Kalman Filter established steady-state standard deviations of 0.3, 0.4, and 0.4 arcseconds, 1σ, in roll, pitch, and yaw respectively. The NGST integrated simulation features a switch to disable the Kalman Filter and simply inject noise with the above values into the position channel of the controller. This feature is provided to improve simulation speed at the expense of fidelity.

The discrete-time, single-axis PID controller equations are of the following form

$$\ddot{\theta}_{cmd} = K_P\theta_{err} + K_I\left(\frac{T_s}{z+1}\right)\theta_{err} + K_D\dot{\theta}_{err}$$

The controller operates at the gyro sampling rate of 10 Hz. Command accelerations are developed using the above expression for the roll, pitch, and yaw channels. The PID gains, K_P, K_I, and K_D, are defined as follows:

$$K_P = \omega_c^2(2f_a\zeta_c^2 + 1)$$
$$K_I = \omega_c^3 f_a\zeta_c$$
$$K_D = \omega_c\zeta_c(f_a + 2)$$
where
$$\omega_c = 2\pi f_c = \text{controller bandwidth (rad/sec)}$$
$$f_c = \text{controller bandwidth (hz)}$$
$$\zeta_c = \text{controller damping ratio}$$
$$f_a = \text{ratio of PD to integral time constants}$$

For the current yardstick design, all three axis use identical parameters: $f_c = 0.025$ Hz, $f_a = 0.075$, $\zeta_c = 0.7071$.

The command accelerations, and command torques to the reaction wheels, are 3x1 vectors containing commands for the roll, pitch, and yaw channels, i.e.

$$\ddot{\theta}_{cmd} = \begin{pmatrix} \ddot{\theta}_x \\ \ddot{\theta}_y \\ \ddot{\theta}_z \end{pmatrix} \quad and \quad \tau_{cmd} = \begin{pmatrix} \tau_x \\ \tau_y \\ \tau_z \end{pmatrix}$$

The command torque is developed via use of the estimated inertia matrix, as shown by the following expression:

$$\tau_{cmd} = \tilde{I}\ddot{\theta}_{cmd}$$

This treatment is necessary for designs such as NGST in which there are significant cross-products of inertia. A completely de-coupled design would be insufficient for such a structure, but might suffice for more symmetric designs.

The roll, pitch, and yaw command torques are filtered via discrete-time elliptic lowpass filters. These filters are designed directly via Matlab^{TM} Signal Processing Toolbox commands. For the yardstick design, the roll, pitch, and yaw filters have identical parameters: 3rd order filters with a 0.15 Hz corner, 3db passband ripple, and 35 dB stopband attenuation.

The tuning of the controller is fairly straightforward. The PID gains are set such that the gain margin is at least 12 dB and the phase margin is at least 30 deg. This is done using only rigid body dynamics in the plant model. Following the PID gain selection, the flexible body dynamics are added to the plant, and the cutoff frequencies and orders of the elliptic lowpass filters are determined such that the closed-loop system is gain-stabilized by at least 10 dB. Table II-1 gives the results for the current NGST design. Note that the addition of the lowpass filters has reduced the rigid body upper gain margins and phase margins below the design goals. Through additional tuning of the filter parameters it is possible to completely satisfy these goals, but at this preliminary design stage these margins are sufficient to proceed to the next step, time-domain simulations to predict performance.

Modal Axis	Lower Gain Margin (dB)	Upper Gain Margin (dB)	Phase Margin (deg)	Flexible Mode Gain Suppression (dB)
1	25 @0.0065 hz	10.4 @0.09 hz	22 @0.035 hz	40 @0.42 hz
2	25 @0.0063 hz	10.5 @0.09 hz	22 @0.035 hz	30 @0.51 hz
3	25 @0.0063 hz	10.3 @0.09 hz	22 @0.035 hz	30 @1.1 hz

Table II-1   ACS Controller Stability Margins

There is a final stage to the controller. NGST features a 4-wheel design, but the controller to this point has developed only 3 commands, in body frame. To command the wheels, the pseudo-inverse of the wheel-to-body transformation matrix is used to transform the 3-vector into a 4-vector. The additional degree-of-freedom is controlled by applying a constraint which is used to set the (approximate) mean wheel momentum. This feature may be exploited on-orbit to sweep the wheels as part of a modal survey, and to then bias the wheels to a speed range that avoids structural resonances which adversely affect optical performance. The 4 –vector of wheel torque commands is then given by an expression of the form

$$\tau_{whl} = {}_{wheel}A_{body}^{-1}\tau_{cmd} + \begin{bmatrix} K & 0 & 0 & 0 \\ 0 & K & 0 & 0 \\ 0 & 0 & K & 0 \\ 0 & 0 & 0 & K \end{bmatrix}\left(\frac{H_{max} + H_{min}}{2}\right)$$

where ${}_{wheel}A_{body}$ is the 4x3 wheel-to-body transformation matrix, K is some (small) constant gain, and H_{max} and H_{min} are the maximum and minimum wheel momenta, respectively.

The ACS block includes the reaction wheel disturbance model. The current model neglects all disturbances except for in-plane forces and torques arising from static and dynamic imbalance. A simplfied physical model [9] of this phenomenon is shown in Figure II-2.
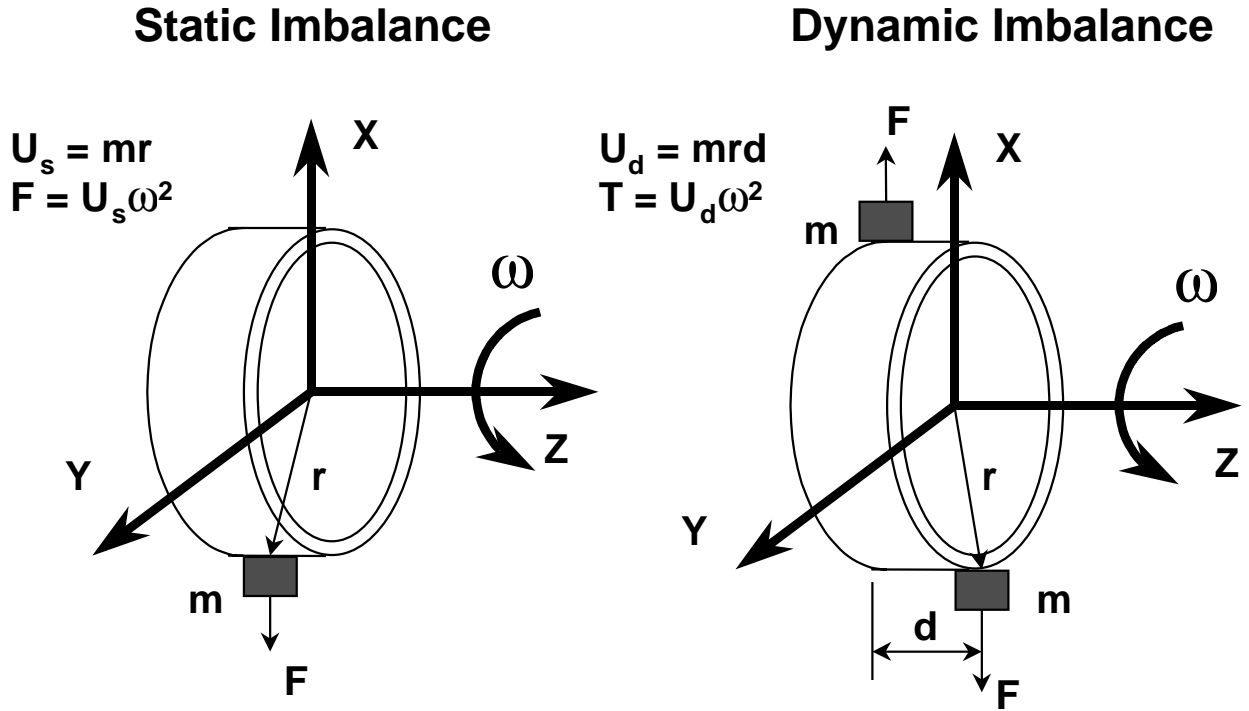
Static Imbalance

$U_s = mr$
$F = U_s \omega^2$

Dynamic Imbalance

$U_d = mrd$
$T = U_d \omega^2$

Figure II-2   Wheel Imbalance Physical Model

These forces and torques are modeled as summations of sinusoidal terms -- the fundamental component at wheel speed plus harmonic and sub-harmonic terms [10] arising from bearing geometry. Equations for this model have the following form, parameterized in terms of static and dynamic imbalance coefficients, harmonic coefficients, and harmonic speed ratios.

$$F_x(t) = U_s \omega^2 \sum_{i=1}^{n} a_i \sin(h_i \omega t + \phi)$$

$$F_y(t) = U_s \omega^2 \sum_{i=1}^{n} a_i \cos(h_i \omega t + \phi)$$

$$T_x(t) = U_d \omega^2 \sum_{i=1}^{n} a_i \sin(h_i \omega t + \phi)$$

$$T_x(t) = U_d \omega^2 \sum_{i=1}^{n} a_i \cos(h_i \omega t + \phi)$$

The parameters for the above expressions used in the NGST model, provided in [10], are taken from measurements on wheels for HST. Similar measurements have been taken on Ithaco wheels, and other sources are being explored to enlarge the database of wheel disturbance models for subsequent analysis.

Using the above model, Representative plots of wheel force time history and power spectral density are given in Figures II-3 and II-4, respectively, for one axis of a single wheel running at 1200 rpm (20 Hz). The time history appears, qualitatively, to show a narrowband noise process. The PSD clearly highlights the harmonic nature of the signal
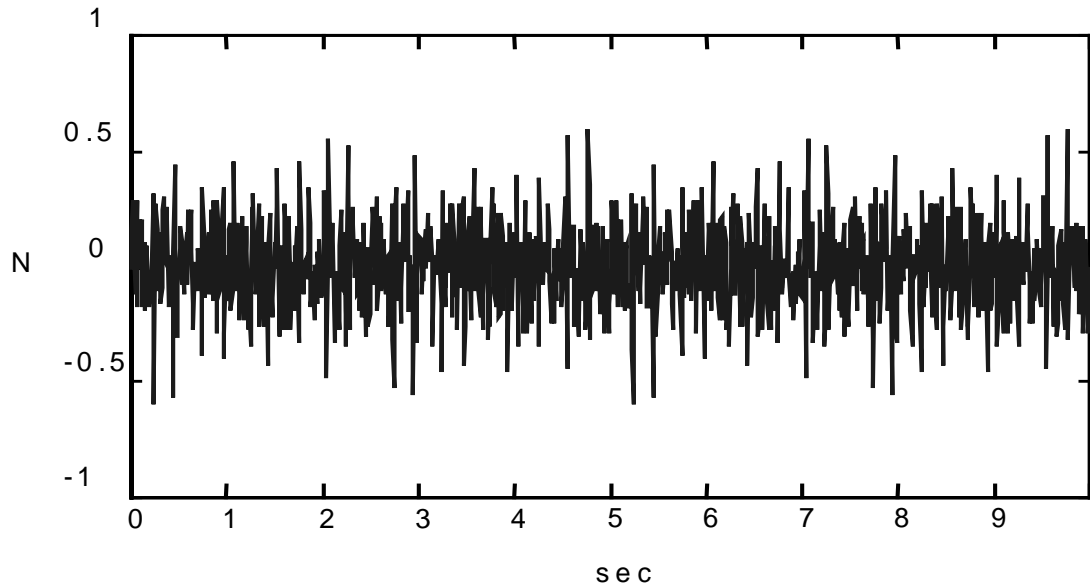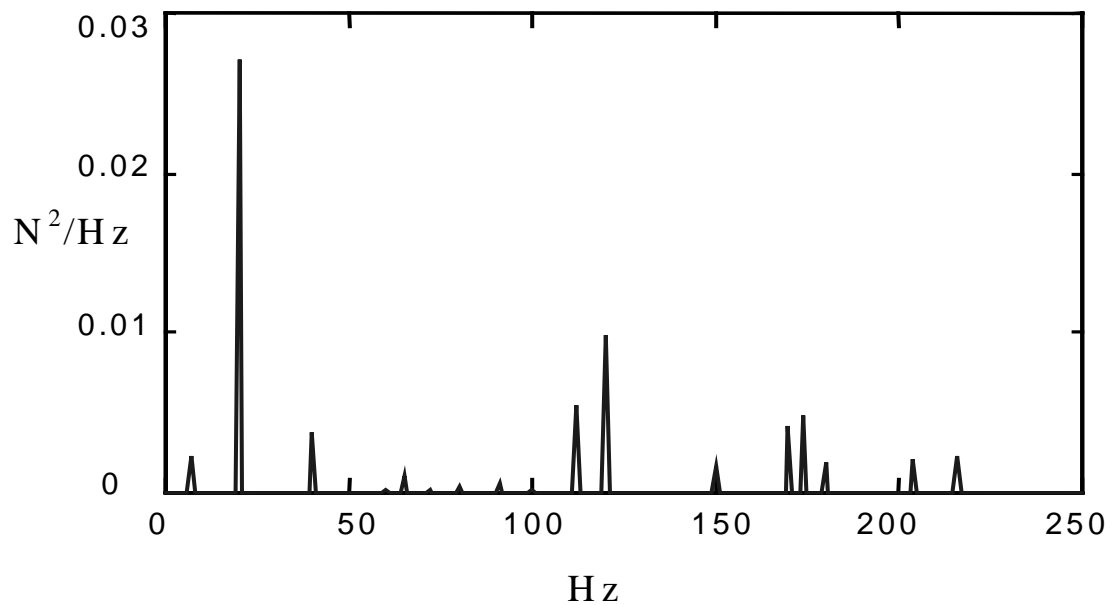

F i g u r e I I - 3   **W h e e l F o r c e v s T i m e**

F i g u r e I I - 4   **W h e e l F o r c e P S D**

The vibration isolation block contains a highly simplified model of a reaction wheel isolation system similar to that discussed in [11,12]. At this time, the isolator is simply modeled as a set of 6 parallel, 2nd order, lowpass filters. Such a model is adequate for frequency-domain analysis, although for the simulation it is still useful to validate the results of the linear analysis. A more realistic model would account for mechanical cross-coupling between the 6 degrees-of-freedom,

A SISO transfer function for this simple filter model is of the form

$$G(s) = \frac{\omega_0^2}{s^2 + 2\zeta_0\omega_0 s + \omega_0^2}$$

The parameters ω_0 and ζ_0 define the characteristics of this filter; ω_0 is the natural frequency, and ζ_0 is the damping. Devices employed in this application may be classified as passive (mechanical spring/damper), hybrid (passive plus electromechanical servo), or active (magnetic suspension). Reasonable assumptions for natural frequency and damping of the filter depend on the device type assumed. Passive devices will exhibit lower damping, typically less than 5-10%, and natural frequencies generally 5 Hz or greater. Hybrid and active devices may be tuned to achieve higher damping, perhaps as high as 50%, and lower natural frequencies, perhaps as low as 0.1 Hz. However, sensor noise and actuator non-linearities will combine to limit performance of these devices.

Figure II-5 shows two representative transfer functions. One represents a 10 Hz, 5 % damped passive suspension; the second represents a 1 Hz, 40% damped hybrid device with ideal feedback sensors (no noise floor at high frequencies).
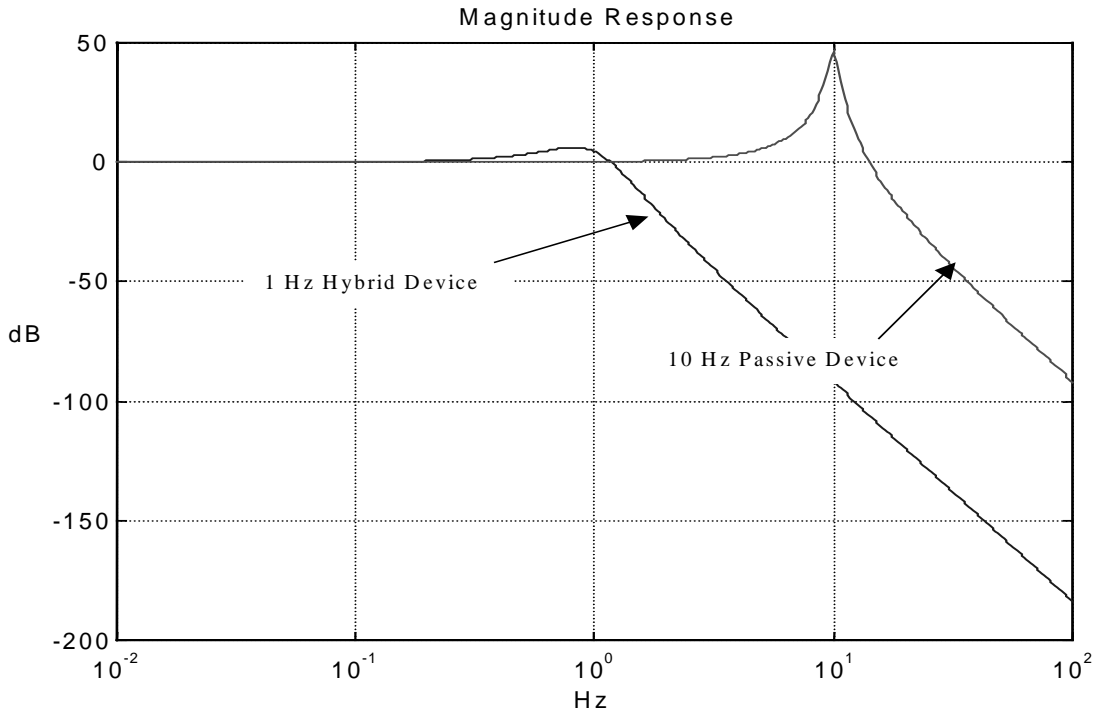

Figure II-5   Sample Isolator Response Functions

III. FINITE ELEMENT AND DYNAMICS MODELS

The mass properties and modal properties, which together are the fundamental quantities in the dynamics block of the integrated system model, are derived from a finite element model of the yardstick design. This FEM, shown in Figure III-1, contains approximately 900 grid points and 5400 degrees-of-freedom. A detailed model of the Optical Telescope Assembly (OTA) was first created, independently of the full observatory model, to study issues such as thermal/structure interactions and optical compensation. For dynamics analysis, the OTA model was combined with highly simplified models for the Spacecraft Support Module (SSM), Integrated Science Instrument Module (ISIM), thermal isolation truss, and sunshield. For now, the sunshield membrane mass has been distributed along the length of the beam elements that model the booms. The remainder of the SSM, ISIM, and truss are simply modeled using concentrated mass and beam elements. Figure III-1 also indicates the locations and grid point numbers of the coordinates whose displacements are required to compute the dynamic and optical quantities required to simulate sensory inputs to the two control loops.
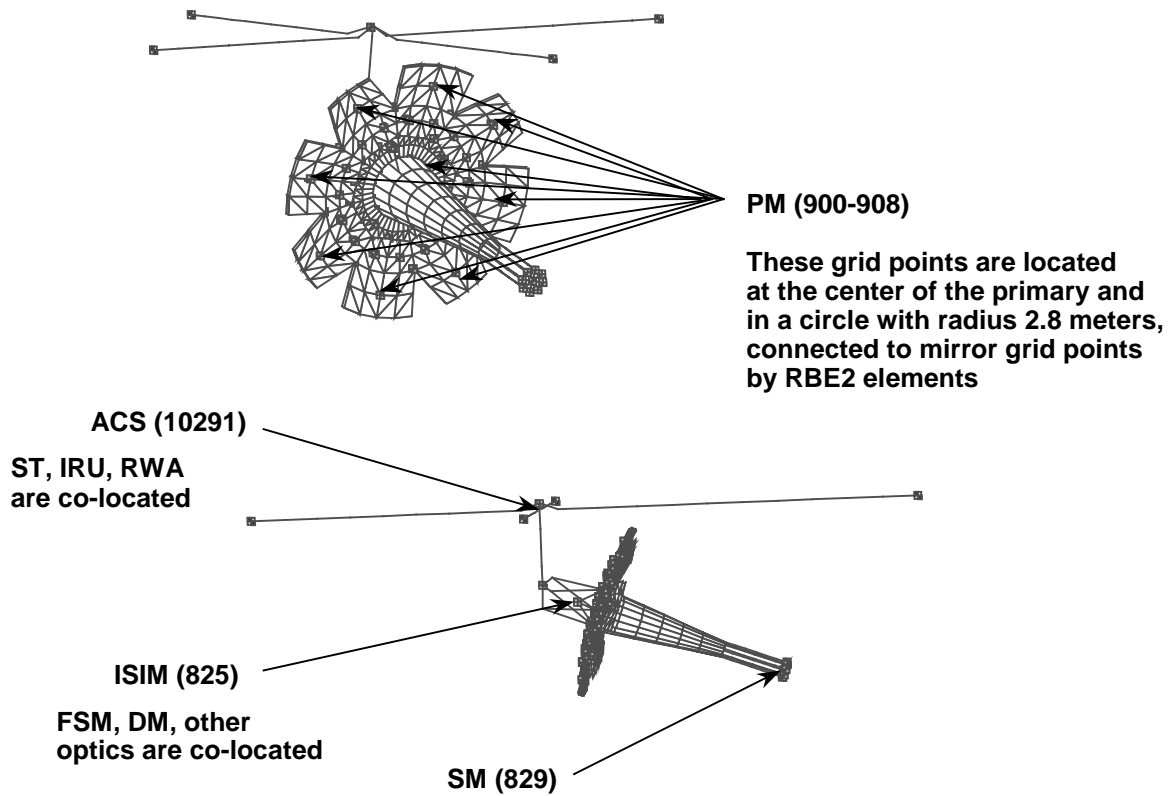

PM (900-908)

These grid points are located at the center of the primary and in a circle with radius 2.8 meters, connected to mirror grid points by RBE2 elements

ACS (10291)

ST, IRU, RWA are co-located

ISIM (825)

FSM, DM, other optics are co-located

SM (829)

Figure III-1   NGST Finite Element Model

The FEM is converted from a NASTRAN bulk data deck into an IMOS input file using *nas2imos*. In Matlab, this IMOS model assembles the mass and stiffness matrices, and an eigenanalysis is performed to extract the desired number of modes. Once the modes and mode shapes are available, and the input and output degrees of freedom are defined, the linear state-space system representation of the flexible body model is computed. The rigid body mass properties are easily extracted from the eigenvector data; the IMOS function *wtcg* provides this information, which is required for the "Rigid Body" block in the dynamics model.

Prior to the extraction of the mass properties and modal data, the following validity checks are performed on the FEM.

- rigid body mode strain energy should be small

- mass properties (total mass, c.g. location, inertia matrix about c.g.) are compared with NASTRAN and hand calculations
- normal modes results are compared with NASTRAN (frequencies, cross orthogonality of modeshapes) and selected frequencies (isolation truss, sunshield, SM truss) are compared with hand calculations
- transient dynamic response is compared with NASTRAN

Structural dynamics in the integrated model framework are modeled by separating the equations of motion into rigid and flexible body components, as shown in Figure III-2. The results are combined to yield the net displacements and rotations necessary to simulate the measurements by gyros, star trackers, and optics. For the dynamics analysis, a simplification is made by essentially assuming that the mirror petals act as rigid bodies. This assumption followed preliminary analysis that indicated the mirror-petal first mode was approximately 400 Hz. Accordingly, the optics models only rely on knowledge of the motions of the 11 grid points identified in Figure III-1.
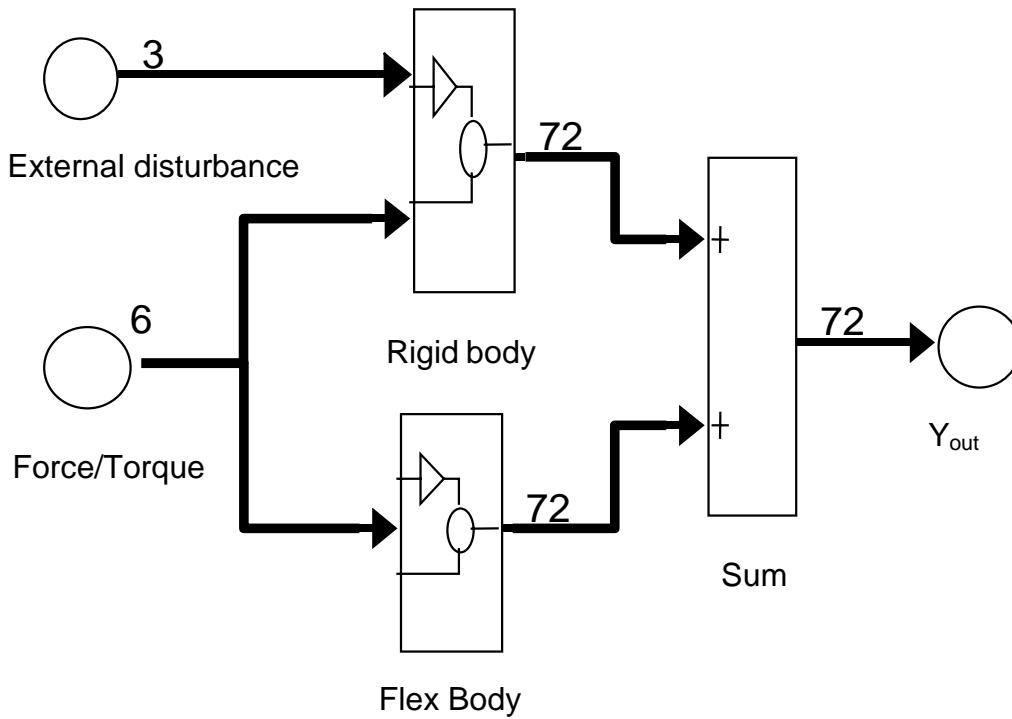

Figure III-2   Dynamics Model Top-Level Block Diagram

The block labeled "Rigid Body" solves Euler's equations of motion for the system about the center of mass.

$$\dot{H} = \sum T - \omega \times H$$

The resulting angular motion may then be used to compute the rigid-body translations of all grid points in the system by virtue of their known displacement vectors relative to the center of mass.

The block labeled "Flex Body" models the flexible dynamics as a linear state-space system, or a series of simultaneous, first-order, linear differential equations in generalized coordinates, i.e.

$$\dot{X} = AX + BU$$
$$Y = CX + DU$$

where the state vector (X), input vector (U), output vector (Y) are defined as follows

$$X = \begin{bmatrix} q \\ \bullet \\ q \end{bmatrix}_{2Nx1}$$

where q is the vector of generalized coordinates, and N is the number of modes extracted in the eigenanalysis

$$U = \begin{bmatrix} f_x & f_y & f_z & \tau_x & \tau_y & \tau_z \end{bmatrix}^T$$

where $f_x, f_y, f_z, \tau_x, \tau_y, \tau_z$ are the reaction wheel forces and torques

$$Y = \begin{bmatrix} y^T_{pm,1} & y^T_{pm,2} & y^T_{pm,3} & y^T_{pm,4} & y^T_{pm,5} & y^T_{pm,6} & y^T_{pm,7} & y^T_{pm,8} & y^T_{pm,9} & y^T_{sm} & y^T_{fsm} & y^T_{acs} \end{bmatrix}^T$$

where Y consists of 12 6x1 vectors, the first 11 of which are the 3 linear and 3 angular displacements of optical surfaces (PM segments 1-9, SM, FSM) and are of the form

$$y_{optics} = \begin{bmatrix} \delta_x & \delta_y & \delta_z & \phi_x & \phi_y & \phi_z \end{bmatrix}^T$$

and the 12th is a 6x1 vector containing the 3 angles and 3 angular velocities sensed by the star trackers and gyros

$$y_{acs} = \begin{bmatrix} \phi_x & \phi_y & \phi_z & \dot{\phi}_x & \dot{\phi}_y & \dot{\phi}_z \end{bmatrix}^T$$

And, finally, the system matrices (A,B,C,D) are given by

$$A = \begin{bmatrix} 0_{NxN} & I_{NxN} \\ diag(-\omega_i^2)_{NxN} & diag(-2\zeta\omega_i)_{NxN} \end{bmatrix}_{2Nx2N}$$

$$B = \begin{bmatrix} 0_{Nx6} \\ \Phi^T_{i,dof \, Nx6} \end{bmatrix}_{2Nx6}$$

$$C = \begin{bmatrix} \Phi^S_{i,optic_{66xN}} & 0_{66xN} \\ 0_{3xN} & \Phi^S_{i,iru_{3xN}} \\ \Phi^S_{i,iru_{3xN}} & 0_{3xN} \end{bmatrix}_{72x2N}$$

$$D = 0_{72x6}$$

where N is the number of modes extracted in the eigenanalysis, ω is the vector of natural frequencies, ζ is the vector of modal damping coefficients, and ϕ is the eigenvector matrix. It is assumed, as a default, that the modal damping is 0.001 for all modes. It is straightforward to modify the A matrix at a later time to change the damping, even on a mode-by-mode basis. This is done in many of the parametric studies performed using the integrated model.

IV. LINEAR OPTICS, FAST-STEERING MIRROR, AND GUIDE STAR SENSOR MODELS

A block diagram of the LOS stabilization loop featuring the FSM and guide star sensor is shown in figure IV-1. Displacements of the FEM grid points associated with the optic surfaces, shown in Figure III-1, are combined with the FSM gimbal angles to create a 74x1 state vector sufficient to calculate metrics such as image centroid and wavefront error. The centroid of the image (assumes a point source along the boresight) is combined with a noise model for the NIR detectors to provide the guiding commands for the FSM. The FSM controller moves the 2-axis mirror to track this image and compensate for dynamic tip/tilt LOS errors.
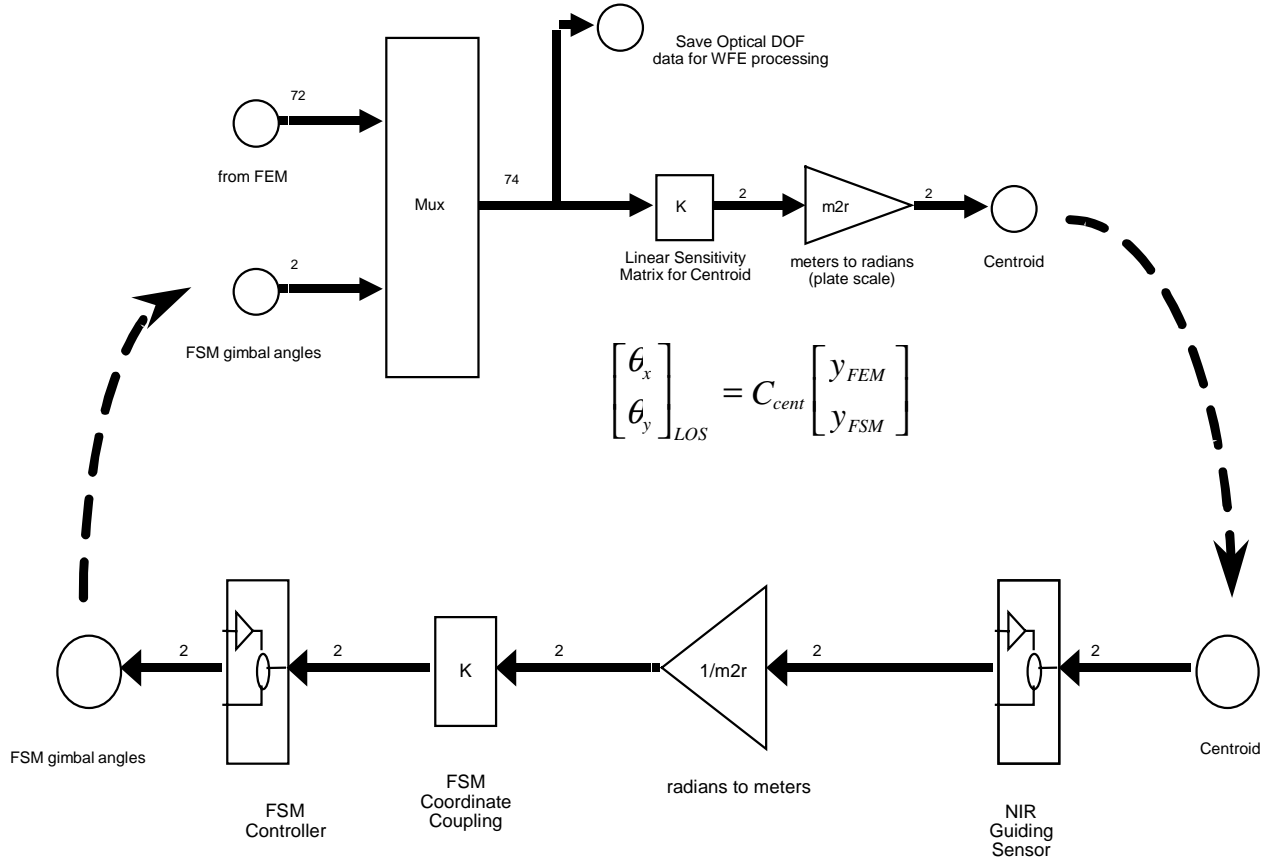

Figure IV-1   LOS Stabilization Loop

Metrics such as centroid and wavefront are computed using linear sensitivity matrices. These are obtained using Matlab and MACOS by introducing a unit perturbation to one degree of freedom at a time and computing partial derivatives of these quantities numerically. The sensitivity matrices are built up one column at a time, with each column corresponding to one of the 74 degrees-of-freedom. Mathematically, the linear optics models are given by

$$C = C_0 + \frac{\partial C}{\partial u} u$$

$$W = W_0 + \frac{\partial W}{\partial u} u$$

where U is the vector of translation and rotations of the FEM coordinates, augmented by the FSM gimbal coordinates (74x1), C is the centroid for the chief ray (2x1), W is the OPD (wavefront) vector (1845x1), $\frac{\bar{o}\,C}{\bar{o}\,u}$ is the centroid linear sensitivity matrix (2x74), and $\frac{\bar{o}\,W}{\bar{o}\,u}$ is the wavefront linear sensitivity matrix (1845x74).

The guide star detector model assumes that the sensor error is essentially due to photon noise. It can be characterized as having a Noise Equivalent Angle that is a function of the detector read noise and quantum efficiency, telescope diameter and throughput, wavelength, and guide star magnitude. The total number of photons collected depends on the detector integration time.

$$NEA = \frac{\sqrt{1 + \frac{R_0}{N}}}{k\sqrt{N}}$$

In this expression, k is the slope of the centroiding function and is given by

$$k = \frac{16D}{3\pi\lambda}$$

And we assume the following values for the remainder of the parameters required:

R0 (detector readout noise over 4 pixels) = 4 * (30 electrons)^2
D (telescope diameter) = 8 m
λ (wavelength) = 2.2 microns
N (total number of detected photons) = $(\varepsilon)(Qe)(\pi D^2/4)(BP)(10^{-0.4M})(\Phi)(T_I)$
ε (throughput) = 0.6
Qe (quantum efficiency) = 0.8
BP (bandpass) = +/- 25%
M (guide star magnitude) = 16.5
Φ (total photon flux) = 3.6x10^{10} photons/m^2/micron/sec
and T_I is the integration time (TBD)

Figure IV-2 shows the sensor noise, in milli-arcseconds, as a function of integration time. To meet a requirement of 5 mas (1s) and allocating no more than 50% of this error to sensor noise, we see that a integration time of at least 0.025 sec (max. 40 Hz sample rate) is required.
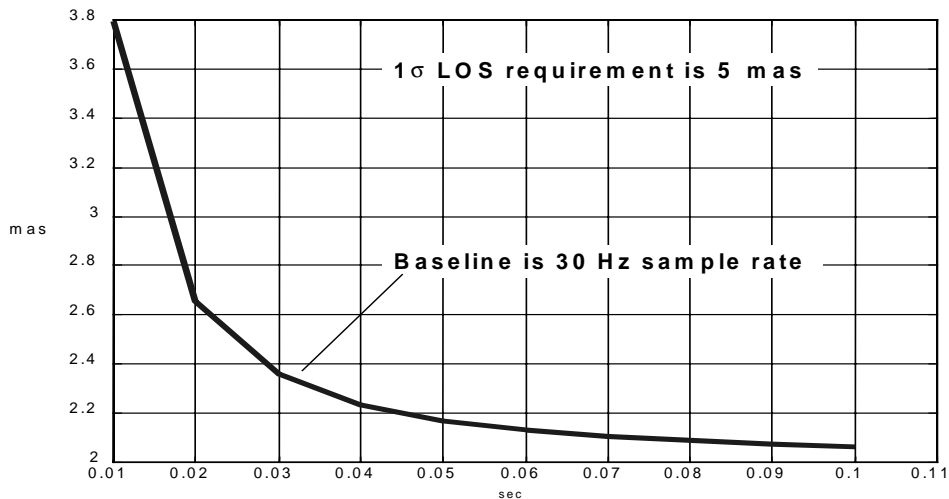

1σ LOS requirement is 5 mas

Baseline is 30 Hz sample rate

Figure IV-2   NEA vs. Integration Time

A discrete-time noise model was developed , allowing the integration time to be varied and appling the correct amount of noise to the X and Y coordinates of the image centroid. Figure IV-3 shows sample time histories of this noise model.
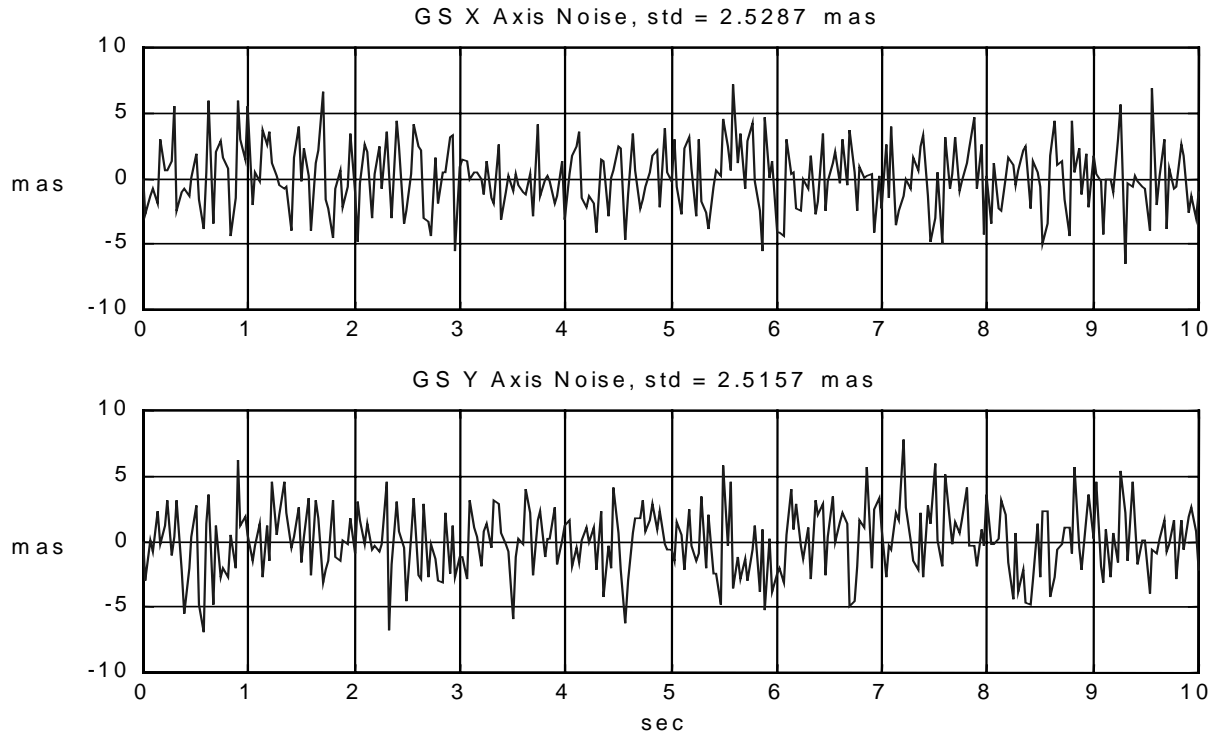

Figure IV-3   GS Noise Model Representative Time Responses

The FSM model was derived from transfer function data taken from an off-the-shelf design [13]. The poles and zeros were scaled from the nominal 2200 Hz rate to the 30 Hz rate set by the guide star noise. A simplified, single-axis representation of the FSM system is shown in Figure IV-4.
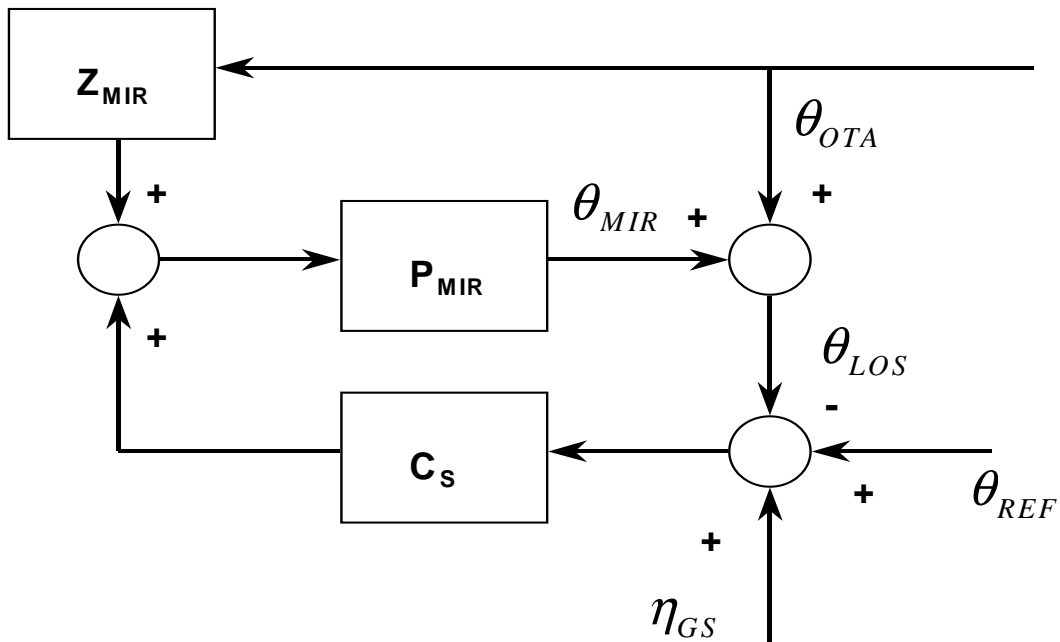

Figure IV-4   FSM Servo Loop Single-axis Block Diagram

The following transfer functions result from the scaled measurements of the LHDC FO50-35 FSM.

$$P_{MIR} = \frac{\omega_0^2}{s^2 + 2\zeta\omega_0 s + \omega_0^2}$$

$$\omega_0 = 2\pi(100); \zeta = 0.02$$

P_{MIR} is neglected in simulation

Z_{MIR} can be neglected

$$C_s = K\frac{s/\omega_1 + 1}{s/\omega_2 + 1}\frac{1}{s/\omega_3 + 1}\frac{1}{s/\omega_4 + 1}$$

$$\omega_1 = 2\pi(0.4); \omega_1 = 2\pi(5.0);$$

$$\omega_3 = 2\pi(0.1); \omega_4 = 2\pi(0.01);$$

$$K = 1000 \quad \text{(includes optical magnification of 120)}$$

The two most important closed-loop transfer functions that can be derived for this system are from guide star noise to LOS error, and from base motion to LOS error. Expressions for these transfer functions are given by

$$\frac{\theta_{LOS}}{\eta_{GS}} = \frac{C_s P_{MIR}}{1 + C_s P_{MIR}}$$

$$\frac{\theta_{LOS}}{\theta_{OTA}} = \frac{1}{1 + C_s P_{MIR}}$$

Plots of these transfer functions are given in Figure IV-5, showing that the FSM servo acts as a low-pass filter to guide star noise, and as a high-pass filter to base motion. The effective bandwidth of this controller (in terms of base-motion suppression) is approximately 2 Hz.
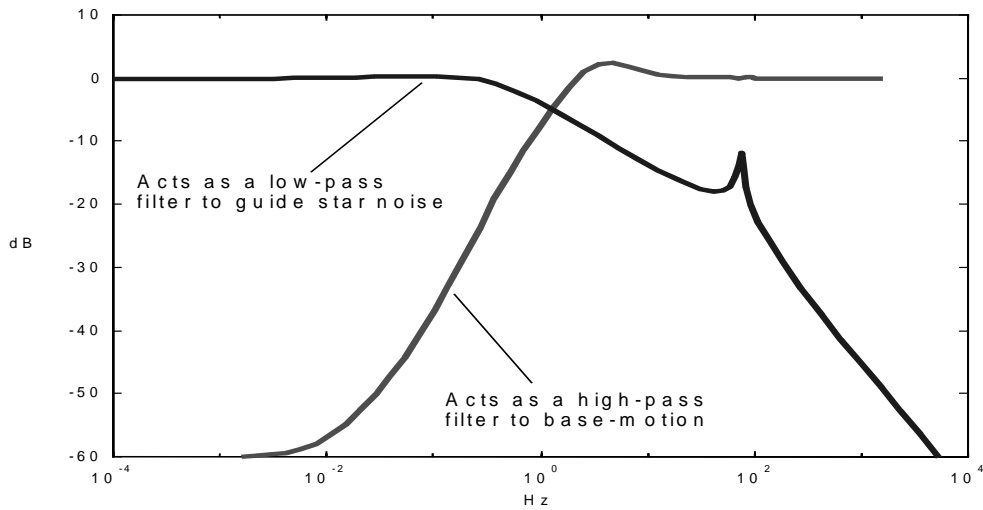

Figure IV-5 FSM Transfer Functions

Figure IV-6 shows the result of the lowpass filter action on the guiding sensor noise time histories shown in Figure IV-3.
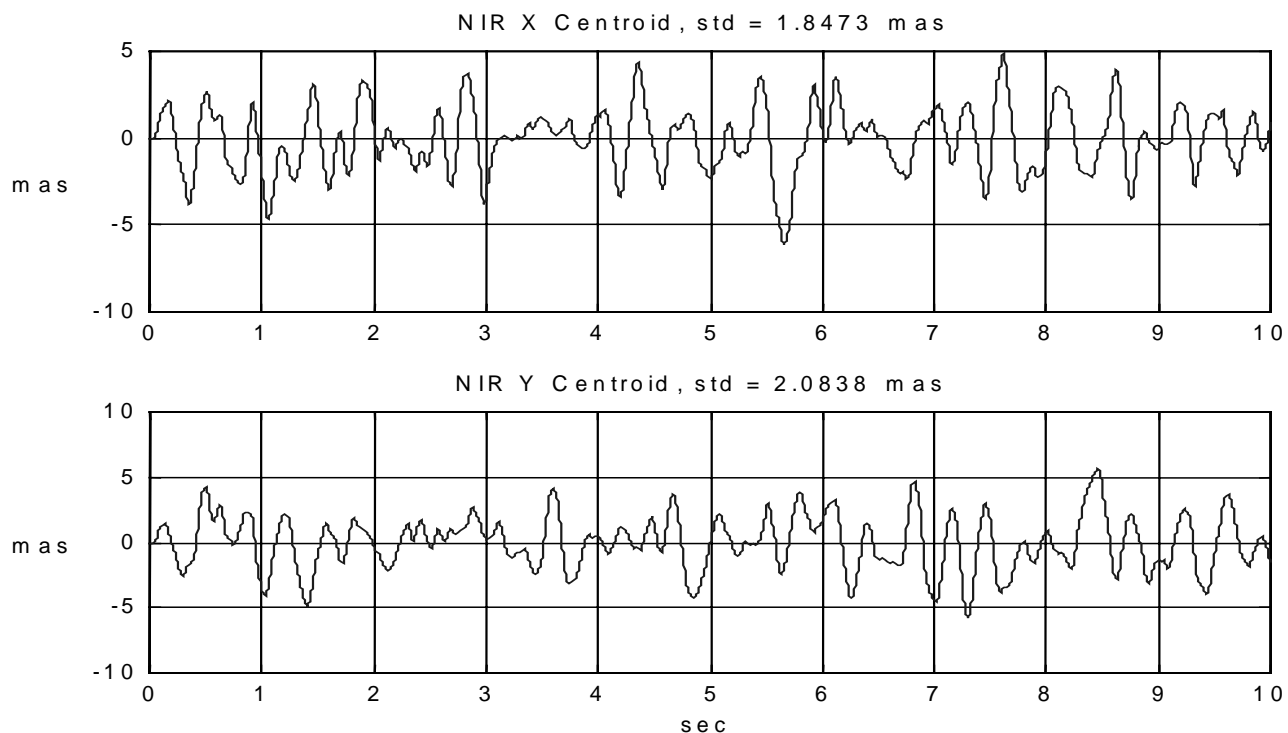
Figure IV-6   Guide Star Noise Floor set by FSM Lowpass Filter Action

This important result represents a limit on LOS performance, which is referred to as the *guide star noise floor*. In the absence of all other disturbance sources, this is the best we can do for this design. The 1-σ LOS error is seen to be 2.785 mas, compared to a 1-σ requirement of 5 mas. In order to provide adequate design margin, it is therefore desirable that the net of all other sources be no larger than the contribution of the guide star noise, such that the R.S.S. remain comfortably below the requirement.

V. REFERENCES

1. Integrated Modeling of Optical Systems User's Manual, Release 2.0, JPL D-13040, November 15, 1995
2. Redding, D.C. and Breckenridge, W.G., "Optical Modeling for Dynamics and Control Analysis," AIAA-90-3383
3. Redding, D.C., Levine, B.M, Yu, J.W., and Wallace, J.K., "A Hybrid Ray Trace and Diffraction Propagation Code for Analysis of Optical Systems," SPIE Vol. 1625, Design, Modeling, and Control of Laser Beam Optics, 1992
4. Mosier, G.E., et.al., "An Integrated Modeling Environment for Systems-level Performance Analysis of the Next Generation Space Telescope," SPIE Vol. 3356, Space Telescopes and Instruments V, 1998
5. Mosier, G.E., et.al., "Fine Pointing Control for a Next Generation Space Telescope," SPIE Vol. 3356, Space Telescopes and Instruments V, 1998
6. Bauer, F.H., Femiano, M.D., and Mosier, G.E., "Attitude Control System Conceptual Design for the X-ray Timing Explorer," AIAA, 1992
7. Murrell, J.W., "Precision Attitude Determination for Multimission Spacecraft," AIAA, 1978
8. Farrenkopf, R.L., "Analytic Steady-State Accuracy Solutions for Two Common Spacecraft Attitude Estimators," Journal of Guidance and Control, Vol. 1, No. 4, July-August 1978
9. Bialke, B., "Microvibration Disturbance Sources in Reaction Wheels and Momentum Wheels," Proc. Conference on Spacecraft Structures, Materials & Mechanical Testing, Noordwijk, The Netherlands, March 27-29, 1996
10. Melody, J.W., "Discrete-Frequency and Broadband Reaction Wheel Disturbance Models," Jet Propulsion Laboratory Interoffice Memorandum 3411-95-200csi, June 1, 1995
11. Spanos, J., Rahman, Z., and Blackwood, G., "A Soft 6-axis Active Vibration Isolator," American Control Conference, Seattle, June 21-23, 1995
12. Spanos, J. and Rahman, Z., "Control Concepts for Active Multi-axis Vibration Isolation," Proc. 6th Intl. Conf. On Adaptive Structures, Key West, Florida, Nov. 13-15, 1995
13. Germann, L. and Lawrence, D., Left Hand Design Corp. white paper for NGST feasibility study, July 1996